IJST EXPLORE International Journal of Science and Technology
CENTRE OF PROFESSIONAL RESEARCH PUBLICATIONS
ISSN 2049-7318

International Journal of Science and Technology Volume 2 No. 1, January, 2013

Large Deformation Behaviour of Continuum Compliant Systems

Theddeus T. Akano, Omotayo A. Fakinlede
Department of Systems Engineering, University of Lagos, Akoka, Lagos. Nigeria

ABSTRACT

Continuum topology of continuous, monolithic compliant mechanisms is designed for finite elastic deformation such that an output port moves in a desired direction when a specified force is applied through an input port. The pseudo-rigid body equivalent of compliant mechanisms (CMs) has been the conventional approach used by earlier researchers to synthesize and analyze compliant mechanisms. Attempts at direct analysis from existing literature are predicted on such assumptions as static linearity or a few times geometric nonlinear conditions. These are justifiable in several situations where compliant systems have been successful in replacing materials with several moving parts. However, the application domain of compliant mechanisms is widening to dynamic environment where the deformations are relatively large. It is therefore necessary to consider nonlinearities resulting from geometry and hyperelasticity. In this paper, methods of continuum mechanics and nonlinear finite element method were deployed to develop model that could capture the behaviour of compliant mechanisms. A hybrid system of symbolic algebra (AceGEN) and a compiled back end (AceFEM) were employed, leveraging both ease of use and computational efficiency. Numerical results using published laboratory investigated compliant mechanisms reveal the deviation that exists with linear and only geometric nonlinear assumptions.

Keywords: *Compliant mechanisms, Hyperelasticity, Nonlinear Finite Element Method, Continuum mechanics, Geometric nonlinearity; Finite Deformation, AceGEN, AceFEM*

1. INTRODUCTION

Compliant mechanisms are defined as mechanical systems that derive some or all of their mobility from the flexibility of one or more of their members. Due to the large-deflection nature of compliant members, analysis and synthesis of such mechanisms are made difficult. One difficulty encountered when designing compliant mechanisms is understanding the deformational characteristics of a flexible continuum. Traditionally, this understanding is gained at the expense of cost-prohibitive, repetitive prototyping and testing. Thus, compliant mechanisms have been limited to applications requiring only simple motions.

Fully compliant mechanisms can be viewed as flexible continua and can be treated as such in their synthesis and analysis (Ananthasuresh and Frecker, 2001). Large and small deformations of a flexible body can be modeled in the body's actual continuum form instead of pseudo-rigid-body models. As such compliant mechanisms can be modeled using the methods of continuum solid mechanics (Ananthasuresh and Frecker, 2001). The basic idea on the design of compliant mechanism is to recast the design problem as an optimal material distribution problem so that the resulting continuum structure can fulfill the requirements of a mechanism and thus, it is called continuum compliant mechanism (Wang and Chen, 2009). Here, we modeled compliant mechanisms using the methods of continuum mechanics. Since the material comprising compliant mechanisms will generally undergo finite strains, displacements, and rotations when the mechanism functions under normal design actuation forces, the analysis and design framework must be general enough to treat finite deformation effects (Swan and Rahmatalla, 2004).

In recent years, the research on the design and analysis of compliant mechanisms has made great progress, at the same time, it has faced many challenges. Compliant mechanisms rely on elastic deformation to achieve force and motion transmission, such deformations are not necessarily small (Howell, 2001). When a structure undergoes sufficiently large deformation, the structure exhibits nonlinear behaviour. This nonlinear behavior comes from two different sources: geometrical and material. The former makes it necessary to include nonlinear terms in the displacement-strain relations and the latter results in the failure of linear material model. Although most successful examples of compliant mechanism design and analysis by nonlinear formulation were reported, most of the designs were based only on nonlinearity due to geometry (Yixian and Liping, 2009; Jinqing and Xianmin, 2011; Bruns and Tortorelli, 2001; Xian et al, 2009; Aten et al, 2012; Joo et al, 2001; Borhan and Ahmadian, 2006; Dinesh and Ananthasuresh, 2007; Akano and Fakinlede, 2011). The use of material model may not be valid in practice because materials with large compliance are often nonlinear materials (Sigmund, 2001a, 2001b). Most engineering materials exhibit nonlinear behaviour when the deformation is sufficiently large. The design and analysis of compliant mechanism

should take the material nonlinearity into account because the functionalities of the complaint mechanism are accomplished from its large deformation (Jung and Gea, 2002).With the present maturity in the analysis of nonlinear materials, the main challenge in its implementation is on the computational efficiency.

Compared to the vast publications on design and analysis of compliant mechanisms with linear materials, very limited works can be cited on nonlinear compliant material behaviour. Swan and Rahmatalla (2004) proposed a methodology for continuum topology design of continuous, monolithic, hinge-free compliant mechanisms and use finite elastic deformation such that an output port region moves in a desired direction when a specified force is applied at an input port region. Swan and Rahmatalla (2005) developed formulation for design of continuous, hinge-free compliant mechanisms. The mechanism was examined within a continuum structural topology optimization framework. The proposed formulation involves solving two nested optimization problems. Bruns and Tortorelli (2001) considered geometric nonlinearity to propose a well-posed topology optimization formulation that leads to convergent mesh-independent results. They account for large deformation of compliant mechanism by using nonlinear elastic analysis in the topology optimization. Jung and Gea (2002, 2004) studied the topology optimization of both geometrically and materially nonlinear structure using a general displacement functional as the objective function. In order to consider large deformation, they expressed the effective stress and strain in terms of 2nd Piola–Kirchhoff stress tensor and Green–Lagrange strain tensor, and constitutive equation is derived from the relation between the effective stress and strain. Compliant mechanisms examples were used to validate their study.

Polymers are predominantly used in the design of compliant mechanisms (Howell, 2001). It is important to use the nonlinear characteristics of polymers to analyse the performance of compliant systems. Thermoplastic polymers like polypropylene exhibit a viscoelastic material response (Mankame and Ananthasuresh, 2004). It has been frequently noted that with certain constitutive laws, such as those of viscoelasticity and associative plasticity, the material behaves in a nearly incompressible manner (Zienkiewicz and Taylor, 2000). The typical volumetric behavior of hyperelastic materials can be grouped into two classes. Materials such as polymers typically have small volumetric changes during deformation and these are incompressible or nearly-incompressible materials (ANSYS, 2007). An example of the second class of materials is foams, which can experience large volumetric changes during deformation, and these are compressible materials. This implies that most polymers are nearly incompressible. In general, the response of a typical polymer is strongly dependent on temperature (Bower, 2010). At low temperatures, polymers deform elastically, like glass, at high temperatures the behaviour is viscous like liquids and at moderate temperatures, they behave like a rubbery solid. Hyperelastic constitutive laws are intended to approximate this rubbery behaviour. Polymers are capable of large deformations and subject to tensile and compression stress-strain curves (Gong and Moe, 2002). The simplest yet relatively precise description for this type of material is isotropic hyperelasticity (Gongand Moe, 2002).Suitable hyperelasticity model is employed to reproduce the elastic responses for the constitutive theory of finite viscoelasticity (Marvalova, 2006).

In this paper, nearly incompressible isotropic hyperelasticity constitutive relation is employed to model finite viscoelasticity characteristic of polymeric compliant mechanisms. The solution methodology involves the finite element discretization of the compliant mechanism. In order to improve the computational efficiency, a hybrid system of symbolic algebra (AceGEN) and a compiled back end (AceFEM) were employed for the implementation of the solution algorithm.

2. BASIC CONTINUUM MECHANICS

The basic compliant mechanism problem is sketched in Fig. 1. It shows the general domain Ω for the design of a mechanism that transforms force applied at the input port to a desired displacement at the output port in an efficient way. The position vector $\boldsymbol{X}$ in the reference position is transformed to $\boldsymbol{x}$ in its current position. u_{in} is the displacement at the input boundary Γ_{in} as a result of the applied force F_{in} at the boundary while F_{out} is a virtual force at the output boundary Γ_{out} specifying the direction of the desired boundary displacement u_{out}. Γ_g is the support boundary.

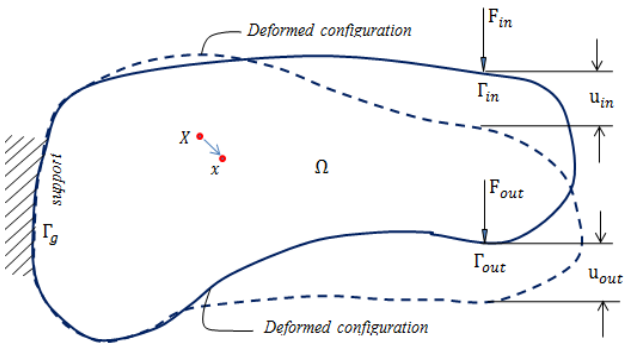

Fig. 1: Deformed continuum compliant mechanism

A bare minimum of fundamental concepts in continuum mechanics are provided here, as theoretical background for large deformations and hyperelastic constitutive material relations. Most, if not all of the information provided in this section have been extensively discussed

in numerous publicly available sources of literature. As a proposed starting point, the interested reader is referred to Holzapfel, 2000; Mase and Mase, 1999 for a quite complete review of continuum mechanics, to Criscione, 2002; Freed, 1995 for a thorough synopsis of natural strain and strain rate, and finally to Bonet and Wood, 1997 for a similar review of the basic concepts of continuum mechanics used in constitutive laws for hyperelasticity.

2.1 Kinematics

A compliant mechanism has material points whose positions are given by the vector $\boldsymbol{X}$ in a fixed reference configuration Ω_r in 2-D space. After the body is loaded each material point is described by its position vector $\boldsymbol{x}$, in the current configuration Ω_c. The position vector in the current configuration is given in terms of its Cartesian components as,

$$\boldsymbol{X} = X_i \boldsymbol{E}_i \tag{1}$$

$$\boldsymbol{X} = X_i \boldsymbol{e}_i \tag{2}$$

$\boldsymbol{E}_i$ and $\boldsymbol{e}_i$ are the unit vectors and summations are implied.

2.2 Cauchy-Green Deformation Tensors

There are two Cauchy-Green Deformation Tensors in the analysis of deformable continuum. We have the right and left Cauchy-Green Deformation Tensors. Right Cauchy-Green tensor is given as,

$$\boldsymbol{C} = \boldsymbol{F}^T \cdot \boldsymbol{F} \tag{3}$$

In the same way, the Left Cauchy-Green Deformation (also known as Finger) tensors is given as,

$$\boldsymbol{b} = \boldsymbol{F} \cdot \boldsymbol{F}^T \tag{4}$$

The Deformation Gradient $\boldsymbol{F}$ is given as,

$$\boldsymbol{F} = \frac{\partial \boldsymbol{x}}{\partial \boldsymbol{X}} \tag{5}$$

The determinant of the deformation gradient is usually denoted by J and is a measure of the change in volume, i.e.,

$$J = det\, \boldsymbol{F}\ ; \quad J^2 = det\, \boldsymbol{C} \tag{6}$$

2.3 Strain Measures

The change in scalar product can be found in terms of the material vectors $d\boldsymbol{X}_1$ and $d\boldsymbol{X}_2$

$$\begin{aligned} \frac{1}{2}\left(d\boldsymbol{x}_1 \cdot d\boldsymbol{x}_2 - d\boldsymbol{X}_1 \cdot d\boldsymbol{X}_2\right) &= \frac{1}{2} d\boldsymbol{X}_1 \cdot \left(\boldsymbol{C} - 1\right) \cdot d\boldsymbol{X}_2 \\ &= \left(d\boldsymbol{X}_1 \cdot \boldsymbol{E} \cdot d\boldsymbol{X}_2\right) \end{aligned} \tag{7}$$

Green (Lagrangian) strain $\boldsymbol{E}$ is then given as,

$$\begin{aligned} \boldsymbol{E} &= \frac{1}{2}\left(\boldsymbol{C} - \boldsymbol{I}\right) = \frac{1}{2}\left(\boldsymbol{F}^T \cdot \boldsymbol{F} - \boldsymbol{1}\right) \\ &= \frac{1}{2}\left(\nabla \boldsymbol{u} + \left(\nabla \boldsymbol{u}\right)^T + \nabla \boldsymbol{u} \cdot \left(\nabla \boldsymbol{u}\right)^T\right) \end{aligned} \tag{8}$$

Index notation:

$$E_{ij} = \frac{1}{2}\left(F_{kl} - \delta_{ij}\right) = \frac{1}{2}\left(\frac{\partial u_i}{\partial X_j} + \frac{\partial u_j}{\partial X_i} + \frac{\partial u_k}{\partial X_j}\frac{\partial u_k}{\partial X_i}\right) \tag{9}$$

Alternatively, the same change in scalar product can be expressed with reference to the spatial elemental vectors $d\boldsymbol{x}_1$ and $d\boldsymbol{x}_2$,

$$\begin{aligned} \frac{1}{2}\left(d\boldsymbol{x}_1 \cdot d\boldsymbol{x}_2 - d\boldsymbol{X}_1 \cdot d\boldsymbol{X}_2\right) &= \frac{1}{2} d\boldsymbol{x}_1 \cdot \left(\boldsymbol{I} - \boldsymbol{b}^{-1}\right) \cdot d\boldsymbol{x}_2 \\ &= d\boldsymbol{X}_1 \cdot \mathbf{e} \cdot d\boldsymbol{X}_2 \end{aligned} \tag{10}$$

Almansi (Eulerian) strain is then given as,

$$\mathbf{e} = \frac{1}{2}\left(\boldsymbol{I} - \boldsymbol{b}^{-1}\right) = \frac{1}{2}\left(\boldsymbol{I} - \boldsymbol{F}^{-T} \cdot \boldsymbol{F}^{-1}\right) \tag{11}$$

2.4 Isotropic Hyperelasticity

Large strain elasticity, or hyperelasticity, is defined in terms of a strain energy function. In order to facilitate the extension of the above equations to the hyperelastic case, the standard theory of isotropic hyperelasticity is briefly reviewed first in this section. Hyperelasticity implies the existence of a strain energy density function Ψ dependent upon the Lagrangian or right Cauchy-Green tensors as

$$\Psi = \Psi\left(\boldsymbol{C}, \boldsymbol{X}\right) = \Psi\left(\boldsymbol{E}, \boldsymbol{X}\right) \tag{12}$$

The second Piola-Kirchhoff stress $\boldsymbol{S}$ tensor now expressed as

$$\boldsymbol{S} = 2\frac{\partial \Psi}{\partial \boldsymbol{C}} = \frac{\partial \Psi}{\partial \boldsymbol{E}} \tag{13}$$

The stress-strain relation could be written as

$$\boldsymbol{C} = \frac{\partial \boldsymbol{S}}{\partial \boldsymbol{E}} = 2\frac{\partial \boldsymbol{S}}{\partial \boldsymbol{C}} = 4\frac{\partial^2 \Psi}{\partial \boldsymbol{C}\partial \boldsymbol{C}} \quad (14)$$

3. METHODOLOGY

Finite element implementations of nearly incompressible material models often employ decoupled numerical treatments of the dilatation, $U(J)$ and deviotoric, $\Psi(\boldsymbol{C})$ parts of the deformation gradient (Sun et al, 2008). The strain energy density function for such a material is decoupled as

$$\Psi(\boldsymbol{C}) = \Psi(\bar{\boldsymbol{C}}) + U(J) \quad (15)$$

Where

$$\Psi(\bar{\boldsymbol{C}}) = \frac{1}{2}\mu(tr\boldsymbol{C} - 3) \quad (16)$$

$$U(J) = \frac{1}{2}k(J-1)^2 \quad (17)$$

k and μ are the material properties known as bulk and shear modulus respectively.

$$\boldsymbol{C} = \boldsymbol{F}^T\boldsymbol{F} \quad (18)$$

$\boldsymbol{F}$ is the deformation gradient and $\boldsymbol{C}$ is Right Cauchy-Green tensor.

Mixed elements are often used to accommodate the volume constrain in incompressible material problem. They are designed to model fully or nearly incompressible hyperelastic materials. For a hyperelastic model that can have multiple deformations state for the same stress level, the penalty factor and the use of Lagrangian multipliers might not be most adequate. It is convenient to use a three-field mixed Hu-Washizu variation form to overcome volumetric locking (Wriggers, 2010). Assuming an independent approximation of the displacement u, the hydrostatic pressure p and the volumetric change parameter θ, a variational form for the finite deformation hyperelastic problem is given by (Mathisen et al, 2011)

$$\Pi(\mathrm{u}, p, \theta) = \int_{\Omega}\left[\Psi(\bar{\boldsymbol{C}}) + p(J-\theta)\right]dV + \Pi_{ext} \quad (19)$$

Where Π_{ext} is the functional for effects of body forces and surface tractions and p is the mixed pressure in the deformed configuration. It is convenient to make a multiplication split of the deformation gradient into a dilatation part $\boldsymbol{F}^{vol}$ and isochoric part $\boldsymbol{F}^{iso}$.

$$\boldsymbol{F} = \boldsymbol{F}^{vol}\boldsymbol{F}^{iso} \quad (20)$$

Mathisen et al. (2011) defined the two parts as,

$$\boldsymbol{F}^{vol} = J \quad (21)$$

$$\boldsymbol{F}^{iso} = 1 \quad (22)$$

Equation (22) is required for constant volume state. The mixed right Green deformation tensor is expressed as,

$$\delta\bar{\boldsymbol{C}} = \delta\bar{\boldsymbol{F}}^T\bar{\boldsymbol{F}} \quad (23)$$

Where

$$\bar{\boldsymbol{F}} = \left(\frac{\theta}{J}\right)^{1/3}\boldsymbol{F} \quad (24)$$

$\bar{\boldsymbol{C}}$ is the mixed right Green deformation tensor. The variation of Eq. (19) gives,

$$\delta\Pi = \int_{\Omega}\left[\begin{array}{l}\dfrac{\partial \Psi}{\partial \bar{\boldsymbol{C}}} : \delta\bar{\boldsymbol{C}} + \delta p(J-\theta) \\ + p(\delta J - \delta\theta)\end{array}\right]dV + \delta\Pi_{ext} \quad (25)$$

A second Piola-Kirchhoff stress is related to the derivative of the stored energy function through Eq. (26).

$$\bar{\boldsymbol{S}} = 2\frac{\partial \Psi}{\partial \bar{\boldsymbol{C}}} \quad (26)$$

Substituting Eq. (26) into Eq. (19) we have,

$$\delta\Pi = \int_{\Omega}\left[\begin{array}{l}\dfrac{1}{2}\delta\bar{\boldsymbol{C}} : \bar{\boldsymbol{S}} + \delta p(J-\theta) \\ + p(\delta J - \delta\theta)\end{array}\right]dV + \delta\Pi_{ext} \quad (27)$$

The first term in Eq. (27) is the inner virtual work $\delta\Pi_{inner}$ given as,

$$\delta\Pi_{inner} = \int_{\Omega}\left[\frac{1}{2}\bar{\boldsymbol{S}} : \delta\bar{\boldsymbol{C}}\right]dV \quad (28)$$

The variation of the mixed right deformation tensor $\bar{\boldsymbol{C}}$ is given as,

$$\delta\bar{\boldsymbol{C}} = \left(\frac{\theta}{J}\right)^{2/3}\delta\boldsymbol{C} + \frac{2}{3}\left(\frac{\delta\theta}{\theta} - \frac{\delta J}{J}\right)\bar{\boldsymbol{C}} \quad (29)$$

But

$$\delta J = J\boldsymbol{C}^{-1} : \delta\boldsymbol{C} \quad (30)$$

Substituting Eq. (30) into Eq. (29), gives

$$\delta\bar{\boldsymbol{C}} = \left(\frac{\theta}{J}\right)^{2/3}\left[\boldsymbol{I} - \frac{1}{3}\boldsymbol{C}\otimes\boldsymbol{C}^{-1}\right] : \delta\boldsymbol{C} + \frac{2}{3}\frac{\delta\theta}{\theta}\bar{\boldsymbol{C}} \qquad (31)$$

The first term of the integrand in Eq. (27) could be expanded as

$$\begin{aligned}\delta\bar{C}_{IJ}\bar{S}_{IJ} &= \delta\bar{F}_{iI}\bar{F}_{iJ}\bar{S}_{IJ} \\ &= \frac{1}{3}\frac{\delta\theta}{\theta}\bar{F}_{iI}\bar{F}_{iJ}\bar{S}_{IJ} \\ &+\left(\frac{\theta}{J}\right)^{1/3}\left[\delta F_{iI} - \frac{1}{3}\delta F_{jJ}F_{jJ}^{-1}F_{iI}\right]\bar{F}_{iJ}\bar{S}_{IJ}\end{aligned} \qquad (32)$$

The Kirchhoff and Cauchy stresses based on the mixed deformation gradient are related as (Zienkiewicz and Taylor, 2000)

$$\bar{\tau}_{ij} = \bar{F}_{iI}\bar{S}_{IJ}\bar{F}_{jJ} = \theta\bar{\sigma}_{ij} \;\; ; \;\; \bar{\boldsymbol{\tau}} = \frac{1}{\theta}\bar{\boldsymbol{F}}\bar{\boldsymbol{S}}\bar{\boldsymbol{F}}^{T} = \bar{\boldsymbol{\sigma}} \qquad (33)$$

If we also note that

$$\delta F_{jJ}F_{jJ}^{-1} = \delta \mathrm{u}_{j,k}F_{kJ}F_{kJ}^{-1} = \delta \mathrm{u}_{j,k}\delta_{kj} = \delta \mathrm{u}_{j,j} \qquad (34)$$

Substituting Eqs. (33) and (34) into Eq. (32), gives

$$\begin{aligned}\delta\bar{C}_{IJ}\bar{S}_{IJ} &= \frac{1}{3}\left(\frac{\delta\theta}{\theta} - \delta u_{j,j}\right)\bar{\tau}_{ii} + \delta u_{i,j}\bar{\tau}_{ij} \\ &= \frac{1}{3}\frac{\delta\theta}{\theta}\bar{\tau}_{rr} + \frac{\partial\delta u_i}{\partial x_j} + \left(\bar{\tau}_{ij} - \frac{1}{3}\delta_{ij}\bar{\tau}_{rr}\right)\end{aligned} \qquad (35)$$

Equation (35) could be expressed in terms of Cauchy stress using Eq. (33) as

$$\delta\bar{C}_{IJ}\bar{S}_{IJ} = \frac{1}{3}\delta\theta\bar{\sigma}_{kk} + \delta \mathrm{u}_{i,j}\left(\bar{\sigma}_{ij} - \frac{1}{3}\delta_{ij}\bar{\sigma}_{kk}\right)\theta \qquad (36)$$

Substituting Eq. (36) into Eq. (27) gives

$$\begin{aligned}\delta\Pi &= \int_{\Omega}\left[\delta\theta\left(\bar{p} - p\right) + \delta p\left(J - \theta\right)\right]dV \\ &+\int_{\Omega}\left[\delta u_{i,j}\left(\bar{\sigma}_{ij} - \delta_{ij}\bar{p}\right)\theta + p\,\delta J\right]dV + \delta\Pi_{ext}\end{aligned} \qquad (37)$$

Where

$$\bar{p} = \frac{\bar{\sigma}_{ii}}{3} = \frac{1}{3}\mathrm{tr}\bar{\boldsymbol{\sigma}} \qquad (38)$$

The variation of the deformation tensor is also given as (Bonet and Wood, 1997)

$$\delta J = J\mathrm{div}\delta\boldsymbol{u} \qquad (39)$$

Equation (39) simplifies Eq. (37) to

$$\begin{aligned}\delta\Pi &= \int_{\Omega}\left[\delta\theta\left(\bar{p} - p\right)\right]dV \\ &+\int_{\Omega}\delta\varepsilon_{ij}\left[\bar{\sigma}_{ij} + \delta_{ij}\left(\frac{J}{\theta}p - \bar{p}\right)\right]\theta\,dV \\ &+\int_{\Omega}\delta p\left(J - \theta\right)dV + \delta\Pi_{ext}\end{aligned} \qquad (40)$$

3.1 Finite Element Discretization

The current configuration $\boldsymbol{x}$ may be expressed in terms of a displacement $\boldsymbol{u}$ from the reference configuration coordinates $\boldsymbol{X}$ as

$$\boldsymbol{x} = \boldsymbol{X} + \boldsymbol{u} \qquad (41)$$

The reference coordinate and displacement field are approximated by isoparametric interpolations given in Eqs. (42) and (43) respectively.

$$X_i = N_r\left(\xi\right)\hat{X}_i^{\,r} \qquad (42)$$

$$u_i = N_r\left(\xi\right)\hat{u}_i^{\,r} \qquad (43)$$

The approximation of the displacement tensor becomes

$$u_{i,j} = N_{r,j}\hat{u}_i^{\,r} \qquad (44)$$

Using the approximations of Eqs. (42) and (43) the matrix form of Eq. (40) becomes

$$\begin{aligned}\delta\Pi &= \delta\hat{\boldsymbol{u}}^{T}\int_{\Omega}\boldsymbol{B}_u^{\,T}\breve{\sigma}\theta dV + \delta\hat{\boldsymbol{u}}_e^{\,T}\int_{\Omega}\boldsymbol{B}_u^{\,T}\breve{\sigma}\theta dV \\ &+\delta\hat{\boldsymbol{P}}^{T}\int_{\Omega}\boldsymbol{N}_p^{T}\left(J - \theta\right)dV \\ &+\delta\hat{\theta}^{T}\int_{\Omega}\boldsymbol{N}_\theta^{T}\left(\bar{p} - p\right)dV + \delta\Pi_{ext}\end{aligned} \qquad (45)$$

Where $\boldsymbol{B}_u$ is the strain displacement matrix given by

$$\boldsymbol{B}_u = \begin{bmatrix} \frac{\partial N_r}{\partial \mathrm{x}_1} & \frac{\partial N_r}{\partial \mathrm{x}_2} & 0 \\ 0 & \frac{\partial N_r}{\partial \mathrm{x}_2} & 0 \\ \frac{\partial N_r}{\partial \mathrm{x}_2} & \frac{\partial N_r}{\partial \mathrm{x}_1} & 0 \end{bmatrix} \tag{46}$$

$$\breve{\boldsymbol{\sigma}} = \bar{\boldsymbol{\sigma}} + \left(\frac{\mathrm{J}}{\theta} p - \bar{p} \right) \mathbf{m} \tag{47}$$

$\bar{p}$ and $\mathbf{m}$ are the mean stress and the mean matrix operator respectively, given as

$$\bar{p} = \frac{1}{3} \mathbf{m}^T \bar{\boldsymbol{\sigma}} \quad ; \quad \mathbf{m} = [1,1,0]^T \tag{48}$$

3.2 Tangent Stiffness

Linearization of Eq. (25) using the Gâteaux derivative may be assembled as

$$\begin{aligned} \Delta(\delta \Pi) = & \int_\Omega \left[\delta \bar{\boldsymbol{C}} : \bar{\boldsymbol{S}} : \Delta \bar{\boldsymbol{C}} + \Delta(\delta \bar{\boldsymbol{C}}) : \frac{\partial \Psi}{\partial \bar{\boldsymbol{C}}} \right] dV \\ & + \int_\Omega p \, \Delta(\delta \mathrm{J}) dV + \int_\Omega \delta p (\Delta \mathrm{J} - \Delta\theta) \, dV \\ & + \int_\Omega \Delta p (\delta \mathrm{J} - \delta\theta) \, dV + \Delta(\delta \Pi_{ext}) \end{aligned} \tag{49}$$

Where $\Delta\theta$, Δp, $\Delta \bar{\boldsymbol{C}}$, ΔJ etc. represent incremental quantities and $\bar{\mathbb{C}}$ is the material tangent moduli given as

$$\bar{\mathbb{C}} = 4 \frac{\partial^2 \Psi}{\partial \bar{\boldsymbol{C}} \partial \bar{\boldsymbol{C}}} = 2 \frac{\partial \boldsymbol{S}}{\partial \bar{\boldsymbol{C}}} \tag{50}$$

Equation (49) could be written in indicial form as

$$\begin{aligned} \Delta(\delta \Pi) = & \int_\Omega \left[\delta \bar{C}_{ij} \bar{\mathbb{C}}_{ijkl} \Delta \bar{C}_{ij} + \frac{1}{2} \Delta(\delta \bar{C}_{ij}) \bar{S}_{ij} \right] dV \\ & + \int_\Omega p \, \Delta(\delta J) dV + \int_\Omega \delta p (\Delta J - \Delta\theta) dV \\ & + \int_\Omega \Delta p (\delta J - \delta\theta) \, dV + \Delta(\delta \Pi_{ext}) \end{aligned} \tag{51}$$

The spatial tangent of a constitutive model of Eq. (50) is denoted by the transformation given as (Taylor, 2000)

$$\bar{\square} = \frac{1}{\theta} \bar{\boldsymbol{F}} \bar{\boldsymbol{F}} \bar{\mathbb{C}} \bar{\boldsymbol{F}}^T \bar{\boldsymbol{F}}^T \tag{52}$$

The inner virtual work of Eq. (51) could be written matrix form as

$$\begin{aligned} & \Delta(\delta \Pi_{inner}) \\ & = \left[\delta \hat{\mathbf{u}}^T, \quad \delta \hat{\mathbf{u}}_e^T, \quad \delta \hat{\boldsymbol{\theta}}^T \right] \begin{bmatrix} \boldsymbol{K}_{\mathrm{uu}} & \boldsymbol{K}_{\mathrm{u}\theta} & \boldsymbol{K}_{\mathrm{up}} \\ \boldsymbol{K}_{\theta \mathrm{u}} & \boldsymbol{K}_{\theta\theta} & -\boldsymbol{K}_{\theta \mathrm{p}} \\ \boldsymbol{K}_{\mathrm{pu}} & -\boldsymbol{K}_{\mathrm{p}\theta} & 0 \end{bmatrix} \begin{bmatrix} \Delta \hat{\mathbf{u}} \\ \Delta \hat{\boldsymbol{\theta}} \\ \Delta \hat{\mathbf{p}} \end{bmatrix} \end{aligned} \tag{53}$$

Equation (53) may be split into the constitutive $\boldsymbol{K}_{ij}^{(\mathrm{c})}$ and geometric $\boldsymbol{K}_{ij}^{(\mathrm{g})}$ parts

$$\boldsymbol{K}_{ij} = \boldsymbol{K}_{ij}^{(\mathrm{c})} + \boldsymbol{K}_{ij}^{(\mathrm{g})} \tag{54}$$

The constitutive tangent terms for symmetric moduli are expressed as

$$\begin{aligned} \boldsymbol{K}_{uu}^{(c)} &= \int_\Omega \boldsymbol{B}_u^T \bar{\boldsymbol{D}}_{11} \boldsymbol{B}_u \theta \, dV \\ \boldsymbol{K}_{u\theta}^{(c)} &= \int_\Omega \boldsymbol{B}_u^T \bar{\boldsymbol{D}}_{12} \boldsymbol{B}_u \boldsymbol{N}_\theta dV = \boldsymbol{K}_{u\theta}^{(c)^T} \\ \boldsymbol{K}_{up}^{(c)} &= \int_\Omega \boldsymbol{B}_u^T \boldsymbol{m} \boldsymbol{N}_p \, J \, dV = \boldsymbol{K}_{pu}^{(c)^T} \\ \boldsymbol{K}_{\theta\theta}^{(c)} &= \int_\Omega \boldsymbol{N}_u^T \bar{\boldsymbol{D}}_{22} \boldsymbol{N}_\theta \theta \, dV \end{aligned} \tag{55}$$

Where

$$\boldsymbol{N}_\theta = \frac{1}{\theta} \boldsymbol{N} \tag{56}$$

and in matrix notation

$$\begin{aligned} \bar{\boldsymbol{D}}_{11} = & \boldsymbol{I}_{dev} \bar{\boldsymbol{D}} \boldsymbol{I}_{dev} - \frac{2}{3} \left(\mathbf{m} \bar{\boldsymbol{\sigma}}_{dev}^T + \bar{\boldsymbol{\sigma}}_{dev} \mathbf{m}^T \right) \\ & + 2 (\bar{p} - \hat{p}) \hat{I} - \left(\frac{2}{3} \bar{p} - \hat{p} \right) \mathbf{m} \mathbf{m}^T \end{aligned} \tag{57}$$

$$\bar{\boldsymbol{D}}_{12} = \frac{1}{3} \boldsymbol{I}_{dev} \bar{\boldsymbol{D}} \mathbf{m} + \frac{2}{3} \bar{\boldsymbol{\sigma}}_{dev} = \bar{\boldsymbol{D}}_{21}^T \tag{68}$$

$$\bar{\boldsymbol{D}}_{22} = \frac{1}{9} \mathbf{m}^T \bar{\boldsymbol{D}} \mathbf{m} - \frac{1}{3} \bar{\mathrm{p}} \tag{59}$$

$\bar{\boldsymbol{D}}$ is the transformation of $\bar{\mathbb{C}}$ given as

$$\overline{\boldsymbol{D}} \rightarrow \overline{\square} = \begin{bmatrix} D_{11} & D_{12} & 0 \\ D_{21} & D_{22} & 0 \\ 0 & 0 & D_{33} \end{bmatrix} \tag{60}$$

and the deviatoric matrix operator $\boldsymbol{I}_{dev}$ and stress $\bar{\boldsymbol{\sigma}}_{dev}$ are given as

$$\boldsymbol{I}_{dev} = \boldsymbol{I} - \frac{1}{3}\mathbf{m} \otimes \mathbf{m} \quad ; \quad \bar{\boldsymbol{\sigma}}_{dev} = \boldsymbol{I}_{dev} : \bar{\boldsymbol{\sigma}} \tag{61}$$

$\boldsymbol{I}$ is the fourth rank unit tensor. $\hat{I}$ is the matrix form of the fourth rank identity tensor

$$\hat{I} = \frac{1}{2}\begin{bmatrix} 2 & 0 & 0 \\ 0 & 2 & 0 \\ 0 & 0 & 1 \end{bmatrix} \tag{62}$$

The geometric tangent term of Eq. (54) is given as

$$\boldsymbol{K}_{uu}^{(g)} = \int_{\Omega} \left(\nabla \boldsymbol{N} : \bar{\boldsymbol{\sigma}} \nabla \boldsymbol{N} \right) dV \tag{63}$$

Where $\nabla \boldsymbol{N}$ is the spatial gradient of the shape function

3.3 Principle of Virtual Work

The principle of virtual work postulates that the external and the internal virtual work are the same.

$$\delta \Pi_{internal} = \delta \Pi_{inertial} + \delta \Pi_{inner} = \delta \Pi_{ext} \tag{64}$$

This means that the internal virtual work stored in the material is equal to the external virtual work done on the material by external forces. If we consider contact force $\boldsymbol{t}$ and body force $\boldsymbol{b}$ as external forces the following relation holds:

$$\delta \Pi_{ext} = \int_{\Omega} \delta \boldsymbol{u}.\boldsymbol{b} \rho \, d\mathrm{V} + \int_{\Gamma} \delta \boldsymbol{u}.\mathbf{t} \, d\mathrm{S} \tag{65}$$

The virtual inertial work resulting from the kinetic energy is given as

$$\delta \Pi_{inertial} = \int_{\Omega} \delta \boldsymbol{u} \cdot \ddot{\boldsymbol{u}} \rho \, d\mathrm{V} \tag{66}$$

The compact form of linearized inner virtual work is obtained with definitions of the deformation-dependent geometric element stiffness matrix $\boldsymbol{k}_g^{\mathrm{e}}\left(\mathbf{u}^{\mathrm{e}}\right)$ and the deformation-dependent material element stiffness matrix $\boldsymbol{k}_m^{\mathrm{e}}\left(\mathbf{u}^{\mathrm{e}}\right)$ from Eq. (54).

$$\begin{aligned} \Delta \delta \Pi_{inertial}^{\mathrm{e}} &\approx \delta \boldsymbol{u}^{\mathrm{e}} \cdot \left[\boldsymbol{k}_g^{\mathrm{e}}\left(\boldsymbol{u}^{\mathrm{e}}\right) + \boldsymbol{k}_m^{\mathrm{e}}\left(\boldsymbol{u}^{\mathrm{e}}\right) \right] \Delta \boldsymbol{u}^{\mathrm{e}} \\ &= \delta \boldsymbol{u}^{\mathrm{e}} \cdot \boldsymbol{k}_t^{\mathrm{e}}\left(\boldsymbol{u}^{\mathrm{e}}\right) \Delta \boldsymbol{u}^{\mathrm{e}} \end{aligned} \tag{67}$$

with the sum yielding the tangential element stiffness matrix $\boldsymbol{k}_t^{\mathrm{e}}\left(\mathbf{u}^{\mathrm{e}}\right)$

3.4 Approximation of Inertial Virtual Work

Besides discretization of inner virtual work, transient mechanical problems also demand discretization of dynamic virtual work. If we approximate the variation of displacements as well as continuous accelerations with the assistance of shape functions according to Eqs. (42) and (43), we get the approximation of virtual work of inertial forces.

$$\delta W_{inertial}^{\mathrm{e}} = \delta \boldsymbol{u}^{\mathrm{e}} \cdot \int_{\Omega} \boldsymbol{N}^T \boldsymbol{N} \rho \, d\mathrm{V} \, \ddot{\boldsymbol{u}}^{\mathrm{e}} = \delta \boldsymbol{u}^{\mathrm{e}} \cdot \mathbf{m}^{\mathrm{e}} \cdot \ddot{\boldsymbol{u}}^{\mathrm{e}} \tag{68}$$

Where

$$\mathbf{m}^{\mathrm{e}} = \int_{\Omega} \boldsymbol{N}^T \boldsymbol{N} \rho \, d\mathrm{V} \tag{69}$$

Then the system mass matrix $\boldsymbol{M}$ is given as

$$\boldsymbol{M} = \bigcup_{\mathrm{e}=1}^{NE} \mathbf{m}^{\mathrm{e}} \tag{70}$$

NE represents the number of elements

3.5 Approximation of Virtual Work of External Loads

The loads acting on a plane element can be divided into loads acting in the field and those acting at the boundaries of the field. Typical loads in the field are gravitational loads whereas actual structural loads are dominated by boundary loads such as pressure. With the help of displacement variation approximation as in Eqs. (42) and (43), a consistent element load vector of volume loads $\boldsymbol{b}$ can be obtained based on external virtual work.

3.5.1 Volume Loads

$$\delta \Pi_{ext}^{\Omega_{\mathrm{e}}} = \delta \boldsymbol{u}^{\mathrm{e}} \cdot \int_{\Omega} \boldsymbol{N}^T \boldsymbol{b} \rho \, d\mathrm{V} = \delta \boldsymbol{u}^{\mathrm{e}} \cdot \mathbf{r}_{\mathbf{p}}^{\mathrm{e}} \tag{71}$$

Where the element vector of volume forces $\boldsymbol{r}_{\mathbf{p}}^{\mathrm{e}}$ is then given as,

$$\boldsymbol{r}_{\mathbf{p}}^{\mathrm{e}} = \int_{\Omega} \boldsymbol{N}^{T} \boldsymbol{b} \rho \, d\mathrm{V} \tag{72}$$

3.5.2 Boundary Loads

The element load vector of element boundary loads $\boldsymbol{t}$ is derived by observation of external virtual work. Here, the boundary Γ can here be divided into four boundaries Γ_{ι} of the element.

$$\delta \Pi_{ext}^{\Gamma e} = \int_{\Omega} \delta \boldsymbol{u}.\boldsymbol{t} \, d\Gamma = \sum_{i=1}^{4} \int_{\Gamma_i} \delta \boldsymbol{u}.\boldsymbol{t} \, d\Gamma_i = \sum_{i=1}^{4} \delta \Pi_{ext}^{\Gamma ie} \tag{73}$$

The approximation of displacement variation of each boundary Γ_{ie} after the Jacobi transformation is given as

$$\delta \Pi_{ext}^{\Gamma_i} = \delta \boldsymbol{u}^{\mathrm{e}} \cdot \boldsymbol{r}_{ni}^{\mathrm{e}} \tag{74}$$

The summation of all correspondingly calculated equivalent loads $\boldsymbol{r}_{ni}^{e}$ for $i = 1,2,3,4$ yields the consistent equivalent loads of an element.

$$\begin{aligned} \delta \Pi_{ext}^{\Gamma} &= \sum_{i=1}^{4} \delta \Pi_{ext}^{\Gamma i} = \sum_{i=1}^{4} \delta \boldsymbol{u}^{e} \cdot \boldsymbol{r}_{ni}^{e} \\ &= \delta \boldsymbol{u}^{e} . \sum_{i=1}^{4} \boldsymbol{r}_{ni}^{e} = \delta \boldsymbol{u}^{e} . \boldsymbol{r}_{n}^{e} \end{aligned} \tag{75}$$

3.6 Nonlinear Elastomechanics Equations of the Continuum Compliant Mechanism

The principle of virtual work can now be approximated in the element plane as

$$\delta \boldsymbol{u}^{\mathrm{e}} \cdot \mathbf{m}^{\mathrm{e}} \ddot{\boldsymbol{u}}^{\mathrm{e}} + \delta \boldsymbol{u}^{\mathrm{e}} \cdot \boldsymbol{r}_{i}^{\mathrm{e}} \left(\boldsymbol{u}^{\mathrm{e}} \right) = \delta \boldsymbol{u}^{\mathrm{e}} \cdot \left(\boldsymbol{r}_{p}^{\mathrm{e}} + \boldsymbol{r}_{n}^{\mathrm{e}} \right) \tag{76}$$

By summing Eq. (76) or explicitly, the vector of internal loads, $\boldsymbol{r}_{i}\left(\boldsymbol{u}\right) = \bigcup_{\mathrm{e}=1}^{NE} \boldsymbol{r}_{i}^{\mathrm{e}} \left(\boldsymbol{u}^{\mathrm{e}} \right)$ with the vector of external loads $\left(\boldsymbol{r}_{p}^{\mathrm{e}} + \boldsymbol{r}_{n}^{\mathrm{e}} \right)$ and the mass matrix $\mathbf{m}^{\mathrm{e}}$, we obtain the system-related spatially discrete formulation of the principle of virtual work,

$$\delta \boldsymbol{u} \cdot \mathbf{M} \ddot{\boldsymbol{u}} + \delta \boldsymbol{u} \cdot \boldsymbol{r}_{i}\left(\boldsymbol{u}\right) = \delta \boldsymbol{u} \cdot \boldsymbol{r} \tag{77}$$

which can be transferred to an initial value problem of non-linear elastodynamics by application of lemma of variation calculus. The problem is defined by the semi-discrete differential equation of motion of the second order.

$$\mathbf{M} \ddot{\boldsymbol{u}} + \boldsymbol{r}_{i}\left(\boldsymbol{u}\right) = \boldsymbol{r} \tag{78}$$

For elastostatic or quasi-static problems of the continuum compliant mechanism, we can formulate the discrete equation of non-linear static equilibrium by neglecting the inertial forces $\mathbf{M} \ddot{\boldsymbol{u}} = \mathbf{0}$.

$$\boldsymbol{r}_{i}\left(\boldsymbol{u}\right) = \boldsymbol{r} \tag{79}$$

4. ILLUSTRATIVE EXAMPLES AND VALIDATIONS

The analysis of compliant mechanisms using the plane stress elements is illustrated with example problems where the goal is to determine the appropriate methodology for the design and analysis of compliant mechanisms. Results from linear, geometric nonlinear and hyperelasticity formulations were compared with experimental results. In order to validate the transient deflection of a compliant link, we compare the simulation results with the experimental results obtained by earlier researchers. Four cases were looked into for this comparative analysis. For the finite element approximation of the above formulations we used 4-node isoperimetric elements. The entire mechanism geometry was built as adequate. The essential and natural boundary conditions were stated. All the finite element codes have been produced by using a hybrid system of symbolic algebra, AceGEN (Korelc, 2011), which has been developed for automatic generation of finite element codes (Korelc, 1997). The computations have been carried out by the compiled back end, AceFEM (Korelc, 2011).

4.1 Compliant Bistable Micromechanism

The experimental setup by Tsay et al. (2005) is shown in Fig.2. The experimental rig consists of vibration isolation platform to separate external vibarations; a micrography system to capture images to be recorded by computer; a workbench where the chip is laid; scanning electronic microscope (SEM) for observation and measurement; power supply system to drive the actuators. The purpose of their experiment was to observe if the micromechanism was bistable and to measure the deflection of the bistable mechanism.

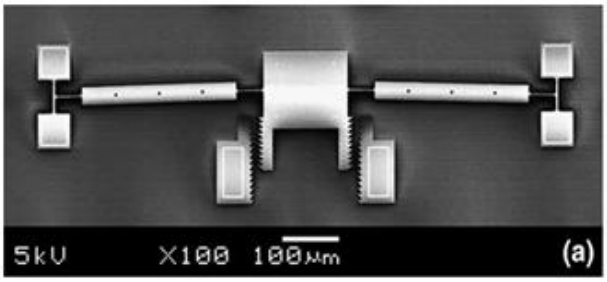

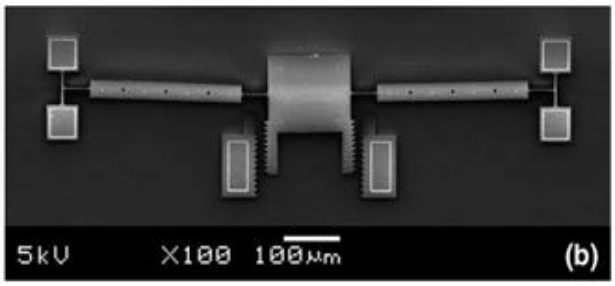

Fig. 2: SEM images of the Compliant Bistable Mechanism switched by a probe.
(a) Before switched; (b) after switched (Tsay et al., 2005)

Figs. 2 (a) and (b) show the images of the compliant bistable micromechanism before and after being switched. After stirred by the probe, the compliant bistable micromechanism switched from the first stable position to the second one and held still. It indicates that the compliant bistable micromechanism functioned as expected. The displacement of central mass was measured by the attached function of SEM.

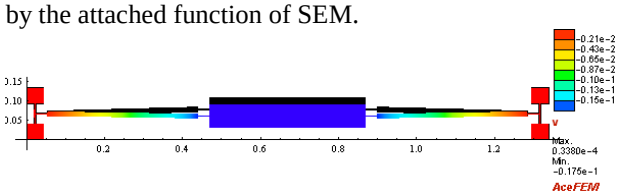

Fig. 3: Deformed and undeformed Complaint Bistable Micromechanism

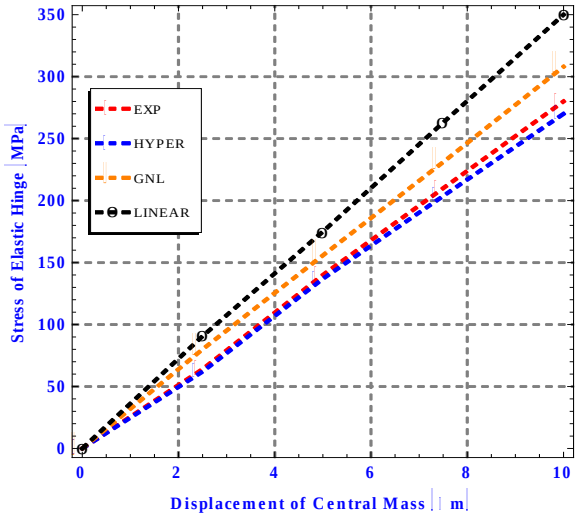

Fig. 4. Stresses of elastic members of Complaint Bistable Micromechanism

The deformed and undeformed positions of this mechanism is shown in Fig. 3 while the displacement of central mass from this experiment is compared with three analysis assumptions; linear, geometric nonlinear and hyperelasticity and shown in Fig. 4.

4.2 Compliant Mechanical Amplifier

Ouyang et al., (2008) conducted the experiment. The prototype Compliant Mechanical Amplifier (CMA) is shown in Fig. 5 (a). In the experimental setup, two PZT actuators (AE0505D16 by Tokin, each has the maximum stroke of up to 16 µm with the maximum output force of 850 N) were installed between two driving links.

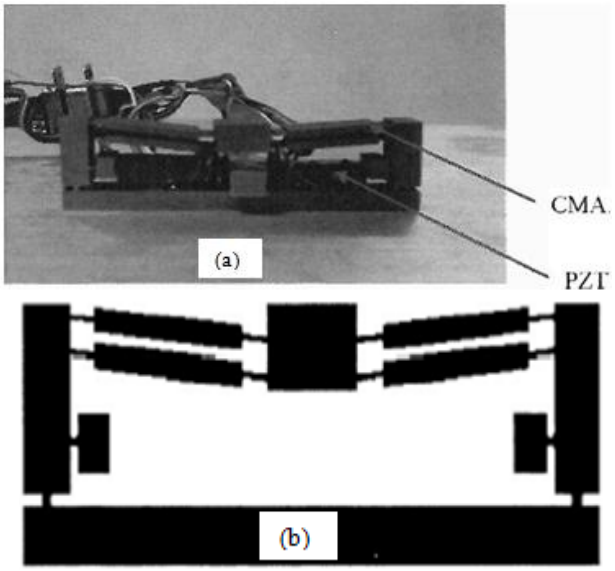

Fig. 5: (a) Prototype of CMA (b) Compliant Mechanical Amplifier (Ouyang et al., 2008)

A controller was designed to provide the control signal to an amplifier (ENV 400, Piezosystem Jena) that was used to supply voltage of about 150 V for the PZT actuators. Strain gauges were glued to two sides of each PZT actuator and acted as a pair to measure the displacement of the PZT actuators. The output displacement of the CMA was captured using an eddy current sensor and recorded by a voltmeter. For static experiments, a dSPACE hardware was used to form the controller. The PZT actuators were driven by PZT amplifiers through controlling the input voltage. The strokes of PZT actuators were measured by strain gauges and then obtained through A/D converter of the dSPACE hardware. The output displacement of the CMA was captured using an eddy current sensor and recorded by a voltmeter. For dynamic experiments, the PZT amplifiers were directly connected with a signal generator of a dynamic analyzer where a pseudorandom signal was generated, and the response of the CMA was sent to the dynamic analyzer for processing.

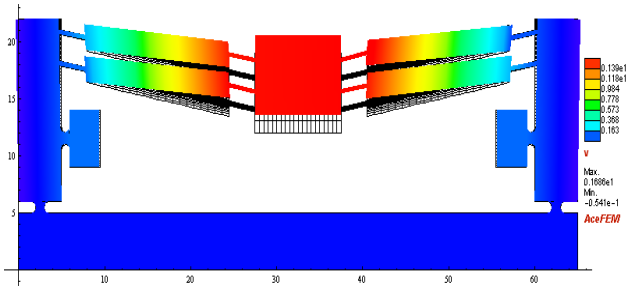

Fig. 6: Deformed and undeformed Complaint Mechanical Amplifier

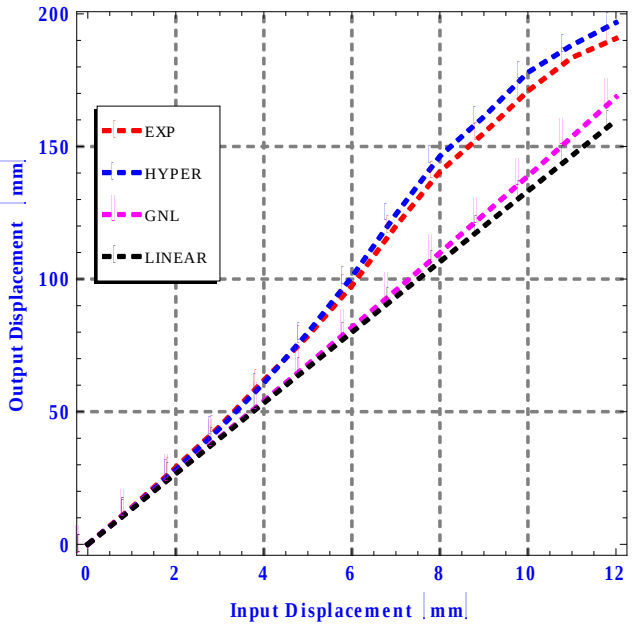

Fig. 7: Output - Input displacement history of the Compliant Mechanical Amplifier

The deformed and undeformed positions of this mechanism are shown in Fig 6. The experimental result is compared with three analysis assumptions: linear, geometric nonlinear and hyperelasticity as shown in Fig. 7.

4.3 Compliant Forceps

Shuib et al. (2007) used the pseudo rigid body method as a methodology to perform the stress analysis of a compliant forceps. They used finite element analysis software, I–DEAS (Integrated Design Engineering Analysis Software) to validate the result from the pseudo rigid body model.

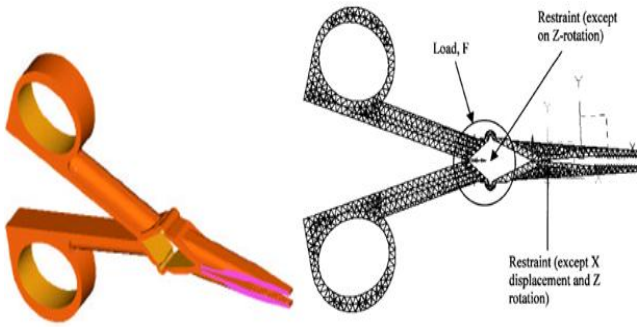

Fig. 8: Compliant forceps and its finite element analysis (Shuib et at., 2007)

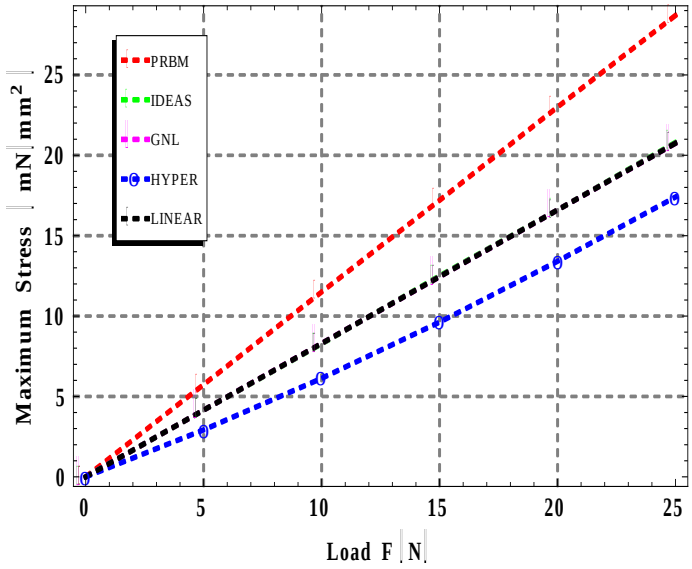

Fig.9: Load verses Maximum stress history of Compliant Forceps

Fig. 8 shows the compliant forceps and its finite element analysis meshing. We extended the analysis to geometric nonlinear and large deformation effects. The comparative analysis result is shown in Fig. 9.

4.4 Compliant Stroke Amplifier

A planar compliant stroke amplifier is described with initial topology, size, shape and boundary conditions (Joo et al., 2001) as shown in Fig. 10.

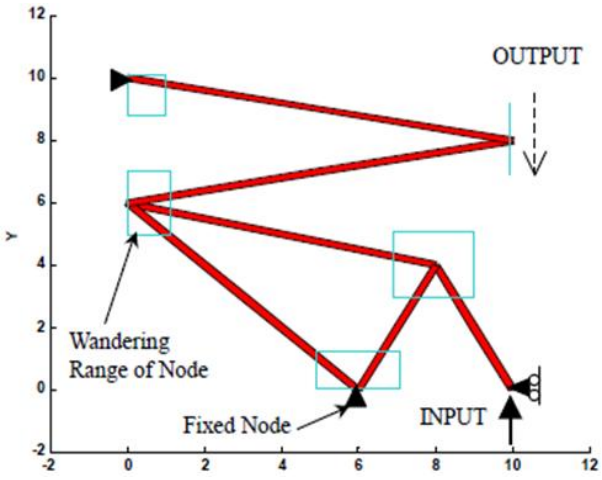

Fig. 10: Problem specification for compliant stroke amplifier design (Joo et al., 2001)

The direction of the desired output motion is out of phase (opposite to input direction) with the input displacement

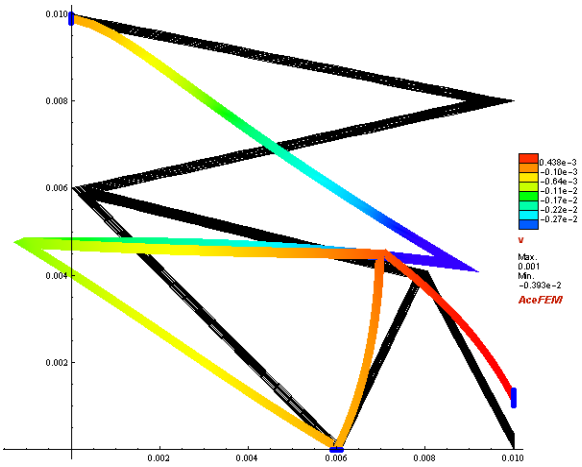

Fig. 11: Deformed complaint stroke amplifier mechanism modeled with all linearity

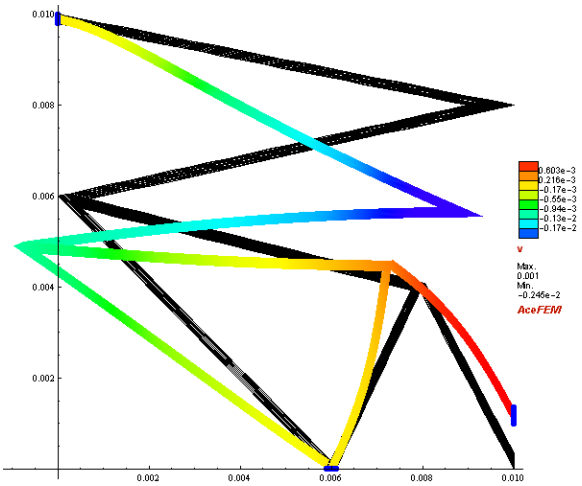

Fig. 12: Deformed complaint stroke amplifier mechanism modeled with geometric nonlinearity (GNL)

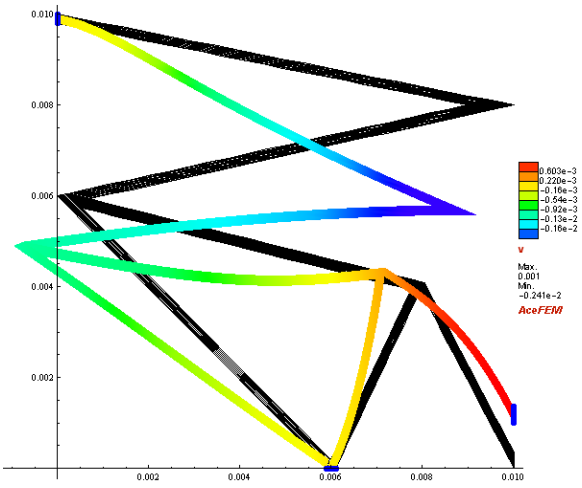

Fig. 13: Deformed complaint stroke amplifier mechanism modeled with hyperelasticity

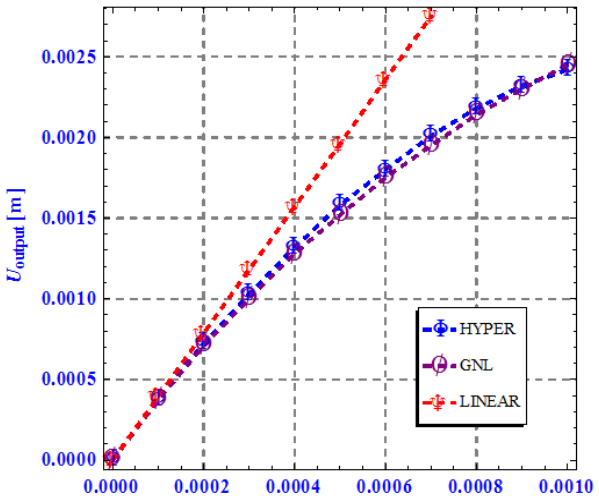

Fig. 14: Output - Input displacement history of complaint stroke amplifier mechanism

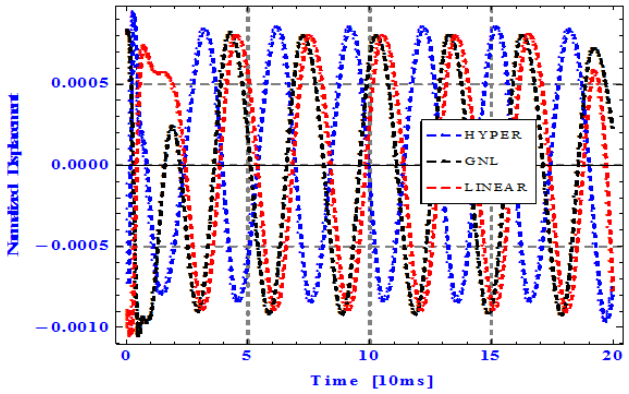

Fig.15: Dynamic response of a compliant link

We analyzed this CM using linear, geometric nonlinear and hyperelasticity assumptions. The deformed and undeformed mechanisms with the respective assumptions are shown in Figs. 11 to 13 while Figs. 14 and 15 show the displacement history and dynamic response of a compliant link respectively.

5. OBSERVATIONS AND DISCUSSION OF RESULTS

Figs. 4 and 9 show the load - stress history of the selected compliant mechanisms. The stress history for each analysis considered differs from that of the experiment. The linear and geometric nonlinear analyses did not show any form of convergence with the experimental results as seen in the case of hyperelasticity. There is a wider range of deviation between the linear model and the experimental results while the results obtained from the geometric nonlinear model displayed a mid-range deviation from the experimental results. The results of the hyperelastic model however are in agreement with that from experiment. We attribute the little discrepancy

between the experimental and the hyperelasticity results to the differences in the device geometry, mainly in the thickness of the compliant mechanism which is highly uncertain due to low fabrication tolerances of micromachining.

The linear and geometric analyses in Figs. 7 and 14, gave a different result pattern from the results obtained in the experiment and finite deformation. However, all the three categories of analyses showed an initial agreement before parting ways at the 3 mm (Fig.7) and 0.2 mm (Fig.14) input displacements. It means that before this deviation, ordinary linear or only geometric nonlinear analysis could capture the deformation behaviour in a given compliant mechanism. Any result obtained after this would not be reliable for any engineering inference.

Fig. 14 shows the dynamic response of a compliant link of the case study compliant mechanism. The dynamic response from GNL and linear models show some agreement in midrange. Hyperelasticity effects become critically important at the end points. Failure may result from these end points despite current analysis in the midrange. This further show why compliant systems that are subjected to large deformations cannot be modeled accurately using linear or only geometrical nonlinear models

6. CONCLUSION

In this paper, we have presented a new methodology for the analysis of compliant mechanisms. We have shown that the choice of either linear or geometric nonlinear analysis is reliable to a certain extent in the deformation behaviour of compliant mechanisms. While geometric nonlinear or even linear model could capture the CM deformation behaviour when input load or displacement is relatively small, results obtained herein have shown that for large input load or displacement, the only reliable result is that from hyperelasticity.

Furthermore, our results have shown that the stress history did not give tolerance for either linear or geometric nonlinear assumptions. Only a hyperelasticity model vividly captures the true stress history of the CM. The understanding of stress behaviour in compliant mechanisms is of much importance since failure could result from improper stress history.

The dynamic response shows that the effects of material nonlinearity become critically important at the end points. Failure may result from these end points.

Therefore, design and analysis of compliant mechanisms considering the effects of both geometric and material nonlinearities is therefore very essentials.

Moreso, integration of numerical and symbolic techniques resulted in a remarkable progress in the applicability, versatility, robustness and efficiency of the algorithm for the solution of the problem.

APPENDIX

AceGen procedure for generating code to work in finite element environment consists of a several steps:

Step 1 – Initialization

- Read of AceGen code generator
  $<<"AceGEN";$
- Select the working environment
  $SMSInitialize["CompliantMechanism", "Environment" \rightarrow "AceFEM"]$
- Select the type of finite element (Q1- 2D four node finite element)
  $SMSTemplate["SMSTopology" \rightarrow "Q1", "SMSSymmetricTangent" \rightarrow True]$

Step 2 – Definition of user subroutine

$SMSStandardModule["Tangent and residual"];$

- Definition of input-output variables
- Kinematics of the selected type of finite element
- Definition of test function
- Definition of governing equations
- Definition of Jacobian matrix
- Definition of stiffness matrix

Step 3 – Definition of output variables using subroutine for postprocessing

$SMSStandardModule["Postprocessing"];$

Step 4 – Generation of code

$SMSWrite[];$

Standard AceFEM procedure consists two basic phase.

1. Phase Data Entry

- phase starts with $SMTInputData[]$
- description of the material model of finite element $(SMTAddDomain)$ defined by code which must be generated before analysis
- mesh generating
  $InputData, SMTAddElement$
- setting boundary conditions
  $SMTAddEssentialBoundary$
- setting loads
  $SMTAddNaturalBoundary$

2. Phase Analysis

- phase starts with *SMTAnalysis*
- solution procedures are executed by the user enters inputs (*SMTConvergence*)
- solving problem by standard Newton-Raphson iterative method
- postprocessing of results as part of analysis

SMTShowMesh or later independently of the analysis *SMTPut*

REFERENCES

[1] Ananthasuresh, G. K.,Frecker, M.,2001.Optimal synthesis with continuum models, in: Howell, L. L., Compliant Mechanisms, John Wiley, New York, pp. 301-335

[2] Wang, M. Y.,Chen, S., 2009. Compliant Mechanism Optimization: Analysis and Design with Intrinsic Characteristic Stiffness,Mechanics Based Design of Structures and Machines: An International Journal, 37 (2), 183 – 200.

[3] Swan, C. C., Rahmatalla,S., 2004. Topological design and nonlinear control of path-following compliant mechanisms, ASME 2004 Design Engineering Technical Conferences and Computers and Information in Engineering Conference, USA, DETC2004-57441.

[4] Howell, L. L., 2001. Compliant Mechanisms, John Wiley & Sons, New York

[5] Yixian,D., Liping, C., 2009. Topology optimization for large-displacement compliant mechanisms using element free galerkin method, International Journal of CAD/CAM, 8 (1), pp. 1-10.

[6] Jinqing,Z., Xianmin,Z., 2011. Topology optimization of compliant mechanisms with geometrical nonlinearities using the ground structure approach, Chinese Journal of Mechanical Engineering, 24.

[7] Bruns., T. E., Tortorelli, D. A., 2001. Topology optimization of nonlinear elastic structures and compliant mechanisms, Computer Methods Appl. Mech. Engrg, 190, pp. 3443 – 3459.

[8] Xian, D. Y.,Ping, C. L., Hua, T. Q., Jia, W. Z., 2009. Topology synthesis of thermomechanical compliant mechanisms with geometrical nonlinearities using meshless method, Advances in Engineering Software, 40, pp. 315–322.

[9] Aten, Q. T.,Jensen, B. D.,Howell, L. L., 2012.Geometrically non-linear analysis of thin-film compliant MEMS via shell and solid elements, Finite Elements in Analysis and Design, 49, pp 70–77.

[10] Joo, J.,Kota, S., Kikuchi, N., 2001. Large deformation behavior of compliant mechanisms, Proceedings of DETC'01 ASME 2001 Design Engineering Technical Conference and Computers and Information in Engineering Conference Pittsburgh, PA.

[11] Borhan, H., Ahmadian,M. T., 2006. Dynamic modeling of geometrically nonlinear electrostatically actuated microbeams: Corotational finite element formulation and analysis, Journal of Physics, International MEMS Conference, DOI:10.1088/1742-6596/34/1/100 Conference Series 34, pp. 606–613

[12] Dinesh,M.,Ananthasuresh, G. K., 2007. A Topology-Optimized Large-Range Compliant X-Y Micro Stage. 13*th* National Conference on Mechanisms and Machines (NaCoMM07), IISc, Bangalore, India, NaCoMM-2007-109.

[13] Akano, T. T., Fakinlede,O. A., 2011.Geometrically nonlinear analysis of compliant mechanism using symbolic numerical approach, International Conference on Innovations in Engineering and Technology (IET), University of Lagos, Nigeria, pp. 519 - 535

[14] Sigmund, O., 2001. Design of multiphysics actuators using topology optimization - Part I: One material structures,Comput. Methods Appl. Mech. Engg.,190 (49-50), Publisher: Elsevier, pp. 6577 – 6604.

[15] Sigmund, O., 2001. Design of multiphysics actuators using topology optimization - Part II: Two material structures, Comput. Methods Appl. Mech. Engg., 190 (49-50), pp. 6605 – 6627.

[16] Jung, D., Gea, H. C., 2002. Compliant mechanism design with non-linear materials using topology optimization,Proceedings of the 2002 ASME Design Engineering Technical Conferences, Montreal, Canada, DETC2002/DAC-34150.

[17] Rahmatall, S., and Swan, C. C.,2005. Sparse monolithic compliant mechanisms using continuum structural topology optimization,Int. J. Numer. Meth. Engng, 62, pp. 1579–1605.

[18] Bruns, T. E., Tortorelli, D. A., 2001. Topology optimization of nonlinear elastic structures and compliant mechanisms," Computer Methods Appl. Mech. Engrg, 190, pp. 3443-3459.

[19] Jung, D., Gea, H. C., 2004. Topology optimization of nonlinear structures, Finite Elements in Analysis and Design, 40, pp. 1417–1427.

[20] Mankame, N., Ananthasuresh,G. K. 2004.A Novel Compliant Mechanism for Converting Reciprocating Translation Into Enclosing Curved Paths, J. Mech. Des., 126 (4), pp 667 – 672.

[21] Zienkiewicz, O. C., Taylor, R. L. 2000. The Finite Element Method. Fifth Edition. Butterworth – Heinemann.

[22] ANSYS Documentation, 2007, http://www.kxcad.net/ansys/ANSYS/ansyshelp/thy_mat5.html.

[23] Bower, A. F., 2010, Applied Mechanics of Solids. CRC Press.

[24] Gong, X. Y., and Moe, R., 2002. On stress analysis for a hyperelastic material,ANSYS Conference.

[25] Marvalova, B., 2006. Application of Comsol Multiphysics 3.2 to finite strain viscoelasticity of an elastomeric solid, Proceedings of the COMSOL Users Conference 2006 Prague.

[26] Holzapfel, G. A. 2000. Nonlinear Solid Mechanics - A Continuum Approach for Engineering, John Wiley & Son, Chichester.

[27] Mase, G. T.,Mase, G.E, 1999. Continuum Mechanics for Engineers, 2nd Edition, CRC Press, New-York.

[28] Criscione, J. C.,2002. Direct tensor expression for natural strain and fast, accurate approximation, Computer ans Strctures, 80 (25), pp. 1895 – 1905.

[29] Freed, A. D., 1995. Natural Strain. J. Eng. Mater. Technol., 117, pp. 379-385.

[30] Bonet, J., Wood, R. D., 1997. Nonlinear Continuum Mechanics for Finite Element Analysis. Cambridge University Press.

[31] Sun, W.,Chaikof, E. L., Levenston,M. E. 2008. Numerical Approximation of tangent Moduli for Finite Element Implementation of Nonlinear Hyperelastic material Models, J Biomech Eng. 130 (6), (7 pages).

[32] Wriggers, P., 2010. Nonlinear Finite Element Methods. Springer-Verlag New York, LLC.

[33] Mathisen, K. M.,Okstad, K. M.,Kvamsdal T.,Raknes, S. B., 2011. Isogeometric analysis of finite deformation nearly incompressible solids,Journal of Structural Mechanics, 44 (3), pp. 260 – 278.

[34] Taylor,R. L.,2000. A mixed-enhanced formulation for tetrahedral finite elements, International Journal for Numerical Methods in Engineering, 47, pp. 205 – 227.

[35] Korelc,J.,AceGEN, AceFEM, 2011, available at http://www.fgg.uni-lj.si/Symech

[36] Korelc,J., 1997. Automatic generation of finite element code by simultaneous optimization of expressions, Theory of Computer Science, 187, pp. 231-248.

[37] Tsay, J., Chang, H., Sung, C., 2005. Design and experiments of fully compliant bistable micromechanisms, Mechanism and Machine Theory, 40, pp. 17–31.

[38] Ouyang, P. R., Zhang, W. J., Gupta, N.M., 2008. A new compliant Amplifier Based on symmetric five-bar topology, Journal of Mechanical Design, ASME, vol. 130/104501-1.

[39] Shuib, S., Yusoff, R., Hassan, A. Y., Ridzwan, M. I. Z., Ibrahim, M., 2007. A disposable compliant-forceps for HIV patients, Journal of Medical Science, 7 (4), pp. 591 – 596.